AN INTELEGENT CONNECTION OF A HYBRID GENERATOR (PV/WIND) TO THE ALGERIAN LOW VOLTAGE ELECTRIC GRID

M.F. ALMI [1, 2], M. ARROUF [1], H.BELMILI [2]

[1] Département de génie électrique, Université de Batna 05000, Algérie
[2] Unité de développement des équipements solaires UDES/Centre de développement des énergies renouvelables CDER, Bou-Ismail, Tipaza 42415, Algérie
almi.mohamed@udes.dz

***Abstract*:** *This paper presents the study and development of micro grid-connected PV/Wind hybrid energy system in Algeria. The aim of this study is to design different configurations and installing the PV/Wind hybrid system with the best quality /price ratio (where it is needed and with the simplest possible configuration). The simplicity of the power system contributes in reducing its maintenance costs and increasing its reliability. For this aim, a new strategy based on the optimization of the energy extracted from these sources, by choosing the best combination location/configuration. Will presented in this work using a low voltage three-phase network to get rid of the storage problem, and with ability to operate in islanding mode to supply consumers with electrical energy in case of electricity shortage resulting from a failure of this latter, and thus limited the number of consumers affected by this network breakdown. These systems could be implemented by, farmers, cooperatives, individuals, and local communities considered as electricity producers in this case. The simulation results show the control performance and dynamic behavior of the PV/Wind system and islanding mode.*

Keywords: *Algeria electricity network, renewable energy, photovoltaic, Wind, smart grid, connection, power system, management.*

1. Introduction

To meet today's society energy needs, it is necessary to find adapted and diversified solutions [1]. Currently, there are basically two possible ways to proceeded; the first is to reduce the receiver's electric energy consumption, and the second method is to find and develop new energy sources and improve their efficiencies. Algeria is the largest natural gas producer and second largest oil producer, after Nigeria, in Africa. Currently, the country is heavily reliant on its hydrocarbon sector, which accounted for almost 70 percent of government budget revenue and grants and about 98 percent of export earnings in 2014, according to the international Monetary Fund [2]. In a country like Algeria, it is not conceivable to abandon hydrocarbons in the production of electricity. But as Algeria has a great solar resource and a modest wind potential, the complementarity of these two sources can be used as hybrid generators (PV/Wind) connected to micro-grid in remote or arid areas where it is profitable (windy and sunny sites).

Thus, we can increase the penetration of renewable energy in electricity generation more profitable way [3].

2. The general configuration of the system

(Figure. 1) displays the hybrid generation system comprising different power sources, as wind turbine generator (WTG), photovoltaic panels (PVs).

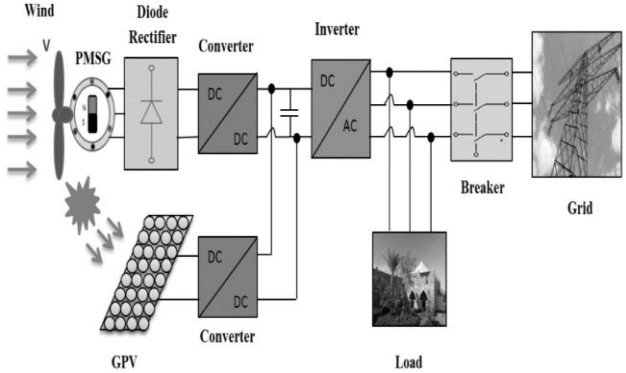

Fig. 1. Illustration of the hybrid (PV/Wind) System used

Mechanical energy from the wind turbine drives the wind generator to generate AC electric power,

which is converted into DC power to form the common DC link. PV array generates DC power. Typically, the DC voltage level from the array is low compared with the adequate level of the DC link necessary to guarantee the excellent operation of the grid interface inverter; thus the DC/DC booster raises the array voltage to a higher level, equivalent to the common DC voltage level. The grid-side inverter changes DC power from wind turbine and PV array into AC power of which voltage and frequency is required for being supplied into the grid.

3. Modeling of Wind generator

3.1 Wind model

The Wind speed can be calculated as [4]:

$$V_v(t) = 10 + 0.2\sin(0.104t) + 2\sin(0.2665t) + \\ + \sin(1.293t) + 0.2\sin(3.6645t) \quad (1)$$

3.2 Wind turbine model

The wind turbine capacity to extract the wind kinetic energy depends on the three factors: the available wind power, the power curve, and the machine behavior to respond to wind speed fluctuation. The mechanical power P_w obtained from a wind turbine is:

$$P_w = \frac{1}{2}.\rho.S_t.C_p(\lambda,\beta).V^3 \quad (2)$$

Where P_w is mechanical output power of the turbine (w); C_p is power coefficient of the turbine; ρ is air density (kg/m3); A is turbine swept area (m^2); v is wind speed (m/s); λ is tip speed ratio and β is blade pitch angle (deg).

A generic equation is used to model $C_p(\lambda,\beta)$. This equation, based on the modelling turbine characteristics is [5]:

$$C_p = 0.73\left(\frac{151}{\lambda_i} - 0.58\beta - 0.002\beta^{2.14} - 13.2\right)e^{-\frac{18.4}{\lambda_i}} \quad (3)$$

$$\lambda_i = \frac{1}{\frac{1}{\lambda - 0.02\beta} - \frac{0.003}{\beta^3 + 1}} \quad (4)$$

The power coefficient expresses the conversion efficiency of the turbine as a function of the tip-speed ratio as:

$$\lambda = \frac{\Omega \times R}{v} \quad (5)$$

Where R is the blade length (m) and Ω is the angular shaft speed (rad/s)

The mechanical torque applied to the wind turbine is given by:

$$T_w = \frac{P_w}{\Omega} \quad (6)$$

3.3 PMSG Model

The voltage equation of a permanent magnet synchronous generator in the d-q reference frame are given by [6]:

$$V_{sd} = -R_s I_{sd} - L_{sd}\frac{dI_{sd}}{dt} + \omega_e L_{sq} I_{sq} \quad (7)$$

$$V_{sq} = -R_s I_{sq} - L_{sq}\frac{dI_{sq}}{dt} - \omega_e L_{sd} I_{sd} + \omega_e \psi_f \quad (8)$$

Where V_{sd}, V_{sq} represent the stator voltages in the d-q axis, I_{sd}, I_{sq} represent the currents in the d-q axis, R_s represents the stator resistance, L_{sd} and L_{sq} represents the d-q axis inductances, $\omega_e = n_p\Omega$ (n_p, number of pole pairs, Ω turbine rotor angular speed) = angle frequency, and ψ_f is the permanent flux linkage.

If the PMSG is a wound rotor machine, which is good for surface mounted applications, the electrical torque of the generator can be expressed as:

$$T_e = \frac{3}{2}n_p[\psi_f I_{sq} + (L_{sd} - L_{sq})I_{sd}I_{sq}] \quad (9)$$

For surface mounted PMSG, we can consider an approximation of $(L_{sd} = L_{sq})$, then torque will.

$$T_e = \frac{3}{2}n_p\psi_f I_{sq} \quad (10)$$

The mechanical equation of PMSG is given by:

$$T_w = j\frac{d\Omega}{dt} + B\Omega - T_e \quad (11)$$

Where T_e is the electromagnetic torque of the generator, j is the generator-rotor inertia and B is the friction constant of the generator.

3.4 MPPT for wind power generator branch

The wind turbine can produce maximum power when the turbine operates at maximum C_p (i.e. at

C_{p_op}). So it is necessary to keep the rotor speed at an optimum value of the tip speed ratio, λ_{opt} [7]. If the wind speed varies, the rotor speed should be adjusted to follow the change.

The target optimum power from a wind turbine can be written as,

$$P_{w\_opt} = \frac{1}{2}.\rho.A.C_{p\_opt}\left(\frac{\Omega_{opt}R}{\lambda_{opt}}\right)^3 = K_{opt}\Omega_{opt}^3 \qquad (12)$$

$$K_{opt} = \frac{1}{2}.\rho.A.C_{p\_opt}\left(\frac{R}{\lambda_{opt}}\right)^3 \qquad (13)$$

$$\Omega_{opt} = \frac{\lambda_{opt}}{R}v = K_w v \qquad (14)$$

Therefore, the target optimum torque can be given by:

$$T_{w\_opt} = K_{opt}\left(\Omega_{opt}\right)^2 \qquad (15)$$

4. Modeling of a PV generator

The module equivalent circuit current I can be expressed as a function of the module voltage V by:

$$I = I_{sc}\left[1 - C_1\left[\exp\left(\frac{V}{C_2.V_{co}}\right) - 1\right]\right] \qquad (16)$$

$$C_1 = \left(1 - \frac{I_{mpp}}{I_{sc}}\right)\exp\left(\frac{-V_{mpp}}{C_2 V_{co}}\right) \qquad (17)$$

$$C_2 = \frac{\left(\frac{V_{mpp}}{V_{co}} - 1\right)}{Ln\left(1 - \frac{I_{mpp}}{I_{sc}}\right)} \qquad (18)$$

Where I_{mpp} is current at maximum power point, V_{mpp} is voltage at maximum power point, I_{sc} is short-circuit current, and V_{oc} is open-circuit voltage of module.

When insolation and temperature changes, the change in above parameters can be calculated using:

$$\Delta T_c = T_c - T_{STC} \qquad (19)$$

$$\Delta I = \alpha_{scT}\left(\frac{G}{G_{STC}}\right)\Delta T_c + \left(\frac{G}{G_{STC}} - 1\right)I_{sc,STC} \qquad (20)$$

$$\Delta V = -\beta_{ocT}\Delta T_c - R_s \Delta I \qquad (21)$$

Where α_{scT} is the current temperature coefficient of the module, and β_{ocT} is the voltage temperature coefficient of the module.

The model translates a reference point to a new point I_{new},V_{new} according (I, V) to the equations below [8].

$$I_{new} = I_{STC} + \Delta I \qquad (22)$$

$$V_{new} = V_{STC} + \Delta V \qquad (23)$$

R_s is calculated from manipulation of $I = f(V)$ characteristics provided by manufacturers at constant temperature. For variations in ambient temperature, T_a , and insolation, the cell temperature, T_c , can be estimated with the linear approximation given by equation:

$$T_c = T_a + \frac{G}{800}\left(NOCT - T_{a,ref}\right) \qquad (24)$$

Where $T_{a,ref}$ is the reference ambient temperature used to specify NOCT.

4.1 MPPT for PV power generator branch

The most commonly used MPPT algorithm is the incremental conductance (INC), due to its ease of implementation in its basic form [9].

IncCond method was implemented in this modelling. If the array is operating at voltage V and current I , the power generation is $P = VI$. At maximum power point, dP/dV should be zero and the sign of dP/dV may be identified by Eq. (26)

$$\frac{dP}{dV} = \frac{d(IV)}{dV} = I + V\frac{dI}{dV} = 0 \qquad (25)$$

$$\frac{dI}{dV} = -\frac{I}{V} \qquad (26)$$

(Fig. 2) shows that the slope of the PV array power curve is zero at the MPP, increasing on the left of the MPP and decreasing on the right hand side of the MPP.

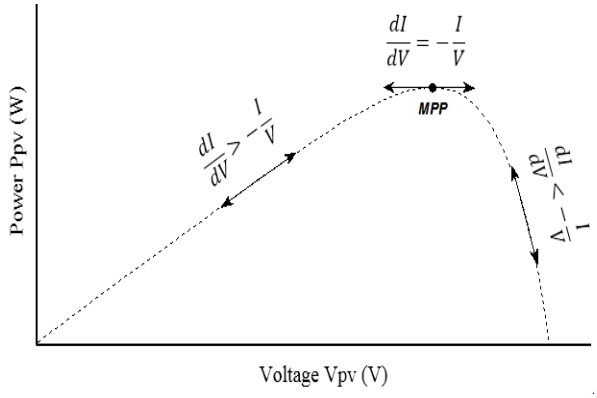

Fig. 2. Graph power versus voltage for INC algorithm

- If $\frac{dI}{dV} = -\frac{I}{V}$ the operating point is at MPP
- If $\frac{dI}{dV} \succ -\frac{I}{V}$ the operating point is at left of MPP
- If $\frac{dI}{dV} \prec -\frac{I}{V}$ the operating point is at right of MPP

5. Modeling of the converters

5.1 Uncontrolled diode bridge rectifier model

In the real machine, the wind speed is constantly varying and so the PMSG produced variable-voltage and variable-frequency output. A three-phase diode rectifier is used to convert the output to dc. Assuming that both the commutating angle and commutating inductance is negligible, the rectifier output voltage and current expression may be simplified and expressed in terms of the peak phase voltage and current (fundamental component) of the generator [10].

$$V_{dc} = \frac{3}{\pi}\sqrt{2}.V_{LL} \tag{27}$$

$$I_{dc} = \frac{\pi}{\sqrt{6}} I \tag{28}$$

Assuming that the output-current of the rectifier is continuous and ripple-free, the dc output power of the rectifier is given by:

$$P_{dc} = V_{dc}.I_{dc} \tag{29}$$

5.2 Boost converter model

The intermediate boost converter produces chopped output voltage and controls the average dc applied to the load [11].

$$V_o = \frac{1}{1-D} V_i \tag{30}$$

The input power of the converter is equal to the output power of the converter if the converter is ideal $(\eta = 1)$, yielding the following equation.

$$I_o = \eta(1-D) I_i \tag{31}$$

Where η is the efficiency of the boost converter, V_o, V_i, are the output and input voltage of the converter, I_o, I_i are the output and input current converter, and D is the duty cycle of the switch

5.3 Inverter modeling

Voltage source inverter (VSI) using pulse width modulation topology is implemented to convert the DC link voltage to AC output voltage. It consists of six insulated gate bipolar-junction transistors (IGBT). Each leg has two IGBT. Furthermore, the SPWM is used in order to generate the gating pulse for applying to the gates of the IGBT [12].

The ratio between the commutation variable vector $[S_a \quad S_b \quad S_c]^T$ and the phase voltage vector $[V_a \quad V_b \quad V_c]^T$ is:

$$\begin{bmatrix} V_{an} \\ V_{bn} \\ V_{cn} \end{bmatrix} = \frac{V_{dc}}{3} \begin{bmatrix} 2 & -1 & -1 \\ -1 & 2 & -1 \\ -1 & -1 & 2 \end{bmatrix} \begin{bmatrix} S_a \\ S_b \\ S_c \end{bmatrix} \tag{32}$$

5.4 LC filter modeling

A state model of a single-phase LC filter is created by using the voltage and current equations, depending on the state variables that are the inductance current i_s capacitor voltage u_c [13].

$$u_m - u_c = i_s R_s + L_s \frac{di_s}{dt} \tag{33}$$

$$i_s - i_r = C \frac{du_c}{dt} \tag{34}$$

The control variable is the input filter voltage u_m as denoted by:

$$\frac{d}{dt}\begin{bmatrix} i_s \\ u_c \end{bmatrix} = \begin{bmatrix} -\frac{R_s}{L_s} & -\frac{1}{L_s} \\ \frac{1}{C} & 0 \end{bmatrix} \begin{bmatrix} i_s \\ u_s \end{bmatrix} + \begin{bmatrix} \frac{1}{L_s} \\ 0 \end{bmatrix} u_m + \begin{bmatrix} 0 \\ -\frac{1}{C} \end{bmatrix} i_r \tag{35}$$

Where the state and command matrix and state variable vector are respectively:

$$A_{p=}\begin{bmatrix} -\frac{R_s}{L_s} & -\frac{1}{L_s} \\ \frac{1}{C} & 0 \end{bmatrix}, B_p = \begin{bmatrix} \frac{1}{L_s} \\ 0 \end{bmatrix}, X_p = \begin{bmatrix} i_s \\ u_c \end{bmatrix} \qquad (36)$$

The filter transfer function is:

$$F_T(s) = \frac{V_c(s)}{V(s)} = \frac{1}{LCs^2 + 1} \qquad (37$$

A three-phase model is derived from this single-phased model using the coupling and decoupling matrix.

5.5 Phase looked loop (Pll)

The phase locked loop, in dependence on the sensed value of the angular frequency ω of the AC source and of the phase position of the AC system voltage, generates a synchronizing signal θ. The synchronizing signal has the importance in synchronizing the dq-reference plane with the AC source voltage abc-system. Thus, when θ_{est} is in synchronism with the phase of the source voltage, the rotating dq-reference plane is locked and maintained in synchronism with the three-phase abc-system [14, 15].

(Fig. 3) shows the classic structure of three phase PLL.

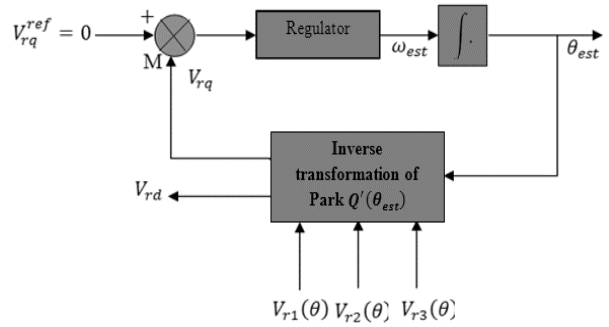

Fig. 3. Detail bloc diagram of PLL

6. Control strategy

Maximum power point tracking (MPPT) controllers are proposed to make the wind and the PV generators work in the maximum power mode that increases the energy captured from the wind speed and the solar radiation. Moreover, adjusted the DC bus bar voltage at the inverter supplying the utility grid.

6.1 Wind control

One the main goals of this part of study is to simplify the structure of the chain of energy conversion dedicated to small capacities' wind turbines. This is necessary to reduce the cost without reducing too much the energy efficiency of the system. The configurations based on a six controlled interrupters bridge rectifier are expensive, involve mechanical measuring devices and require fairly complex control circuit. Here the converter of generator-side is composed of diode rectifier and boost converter, which has the advantages of low cost and simple control. As shown in (Fig. 4), the output voltage of boost converter is V_{bus}, and it is related to duty factor D, mechanical rotational speed ω^*, so generator-side boost converter adopts constant voltage control strategy [7, 16].

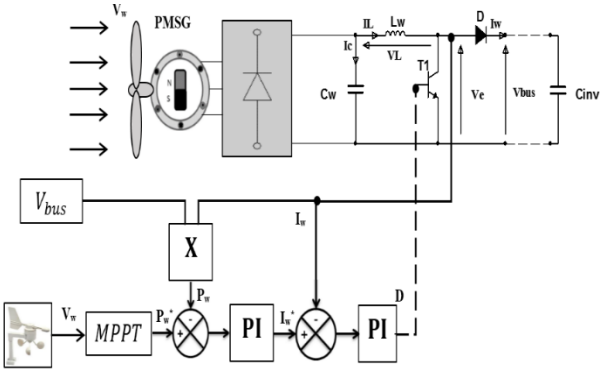

Fig. 4. Control of the wind generator system

6.2 PV control

The controller proposed measuring only the current in the output of the DC/DC converter. Due to the constant DC bus bar voltage in the output of the boost converter, the power can be maximized by maximizing the boost converter output current. This method is simple and suitable for this application [17].

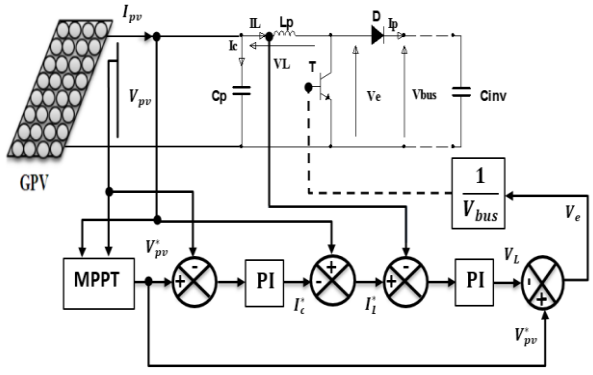

Fig. 5. Control of the PV system

6.3 Grid connection control

It is a command strategy which allows the inverter to control independently the frequency and amplitude of voltage supplied to a load. It is based on the regulation of the voltage (current) in continuous coordinate's dq. Closed control loops used by these controls ensure fast transient response and high steady state performance [18].

The control scheme is presented in (Fig. 8).

6.4 Islanding detection and load shedding

Short circuit can endanger personnel as well as power system and customer equipment. Excessively high or low voltages can also damage equipment. To avoid these damages, protective relays are installed to detect the abnormal condition and to open circuit breaker and isolate the problem. Proper action is generally required within a few fundamental cycles, a time frame that is too fast for central control. For this reason, decisions are often made autonomously by local devices based upon locally available information (e.g. excessive current or out of range voltage)[19 20]. These functions may be performed faster, better, and cheaper with the aid of power electronics or advanced sensors and controllers. This may be especially true if the protective functions can be built into the control systems of distributed generation, as shown in (Fig. 1).

6.4.1 Frequency shift methods

The frequency monitoring is done by PLL park field. Who allows having from the network-estimated voltages, the estimated pulsation ω_{est} is of these two sinusoids very quickly. This estimated pulsation makes it possible to have the estimated frequency by dividing it by 2π the frequency can be thus supervised. It is compared with two thresholds values corresponding to $f_{est} \pm 1\%$.

$$f_{\min threshold} \prec f_{est} \prec f_{\max threshold} \quad (38)$$

$$f_{threshold} = (50 \pm 0.5) Hz \quad (39)$$

The monitoring system activates a temporization if a threshold is crossed during more than 0.1s. The (PV/Wind) hybrid system is isolated from the network thanks to the control switchgear envisaged for this purpose. If the frequency returns between these thresholds values, temporization is given to zero.

6.4.2 Voltage-pulse perturbation method

It is made in the same manner that the frequency. A minimum and maximum threshold is given $U_{abcest} \pm 15\%$.

$$U_{\min threshold} \prec U_{abcest} \prec U_{\max threshold} \quad (40)$$

$$U_{threshold} = (380 \pm 57) V \quad (41)$$

The two RMS voltages are measured. It is necessary that both are below thresholds to start temporization. The same latency time is considered: 0.1s. This monitoring is necessary for an overvoltage or an under voltage.

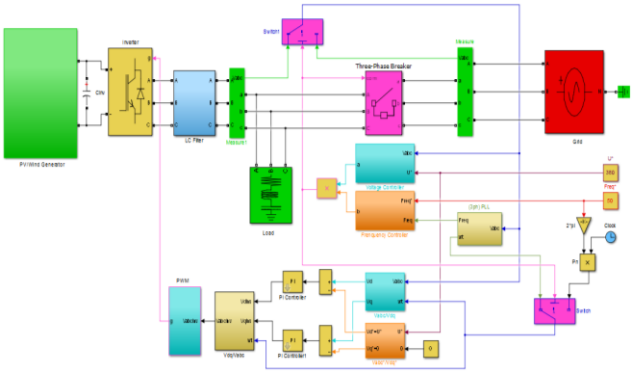

Fig. 6. Grid connection control

7. Simulation results

7.1 Results with (PV/Wind) hybrid system control

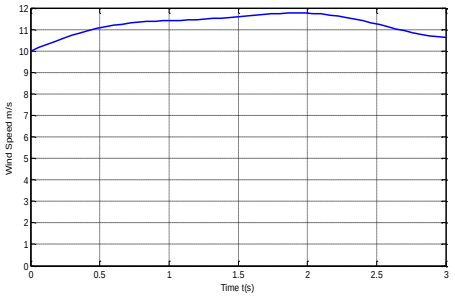

Fig. 7. Wind Speed

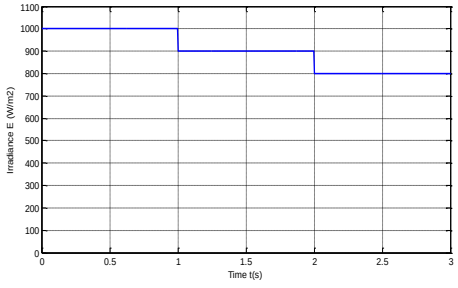

Fig. 8. Solar irradiance

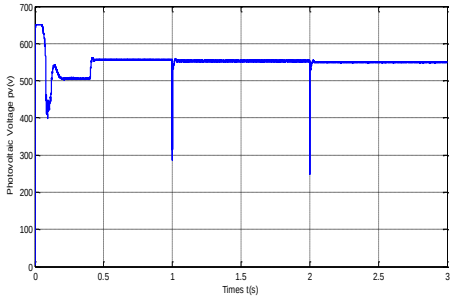

Fig. 9. Photovoltaic voltage

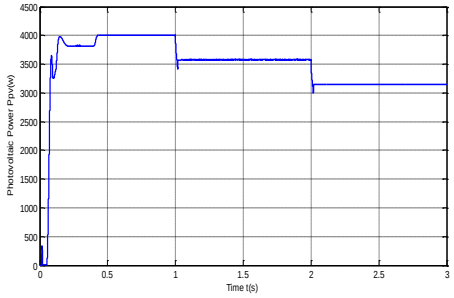

Fig. 10. Photovoltaic power

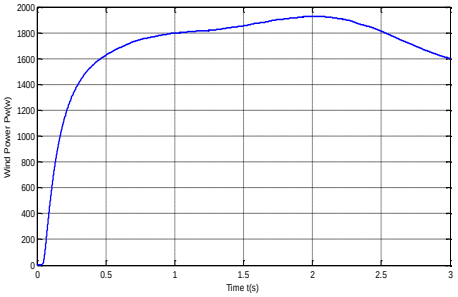

Fig. 11. Wind power

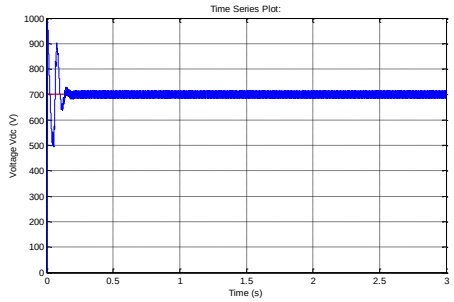

Fig. 12. DC bus voltage

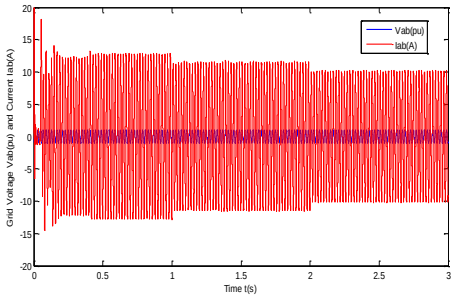

Fig. 13. Grid voltage and current

7.2 Results from islanding system control (with standard conditions)

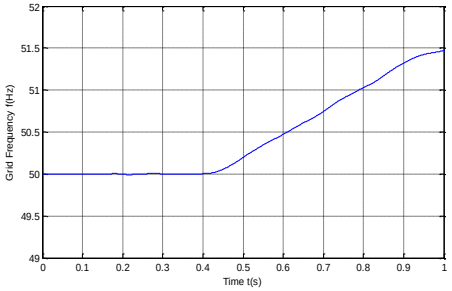

Fig. 14. Grid frequency

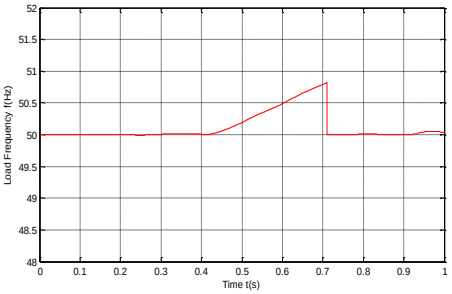

Fig. 15. Load frequency

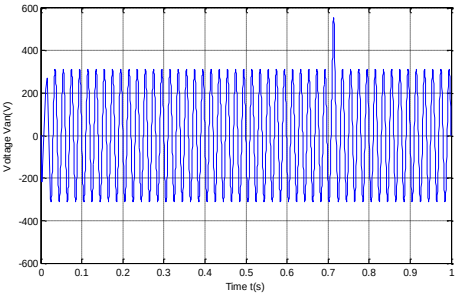

Fig. 16. Load Voltage

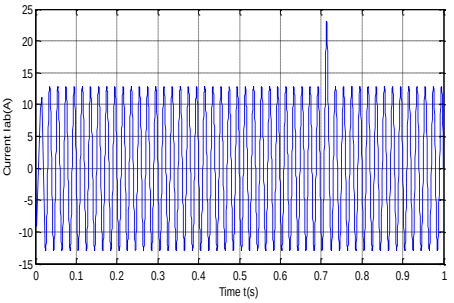

Fig. 17. Load Current

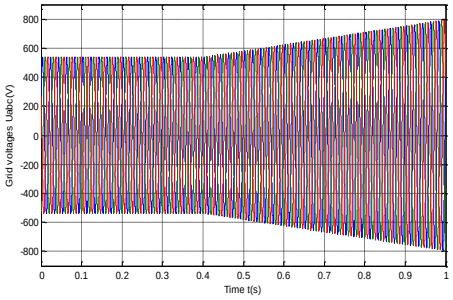

Fig. 18. Grid voltage with overload

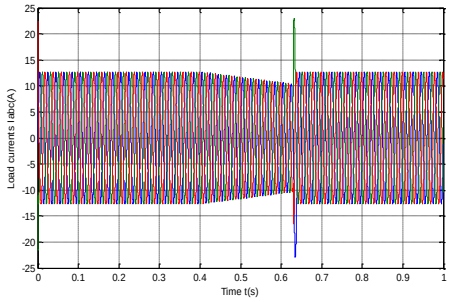

Fig. 19. Load currents with overload

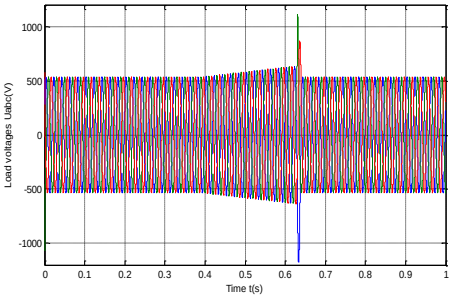

Fig. 20. Load voltage with overload

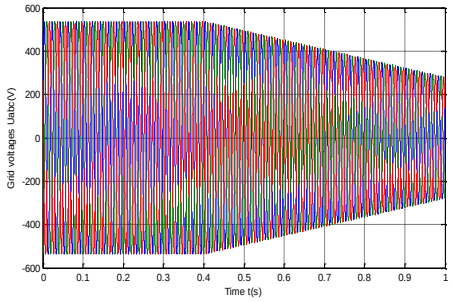

Fig. 21. Grid voltage with under load

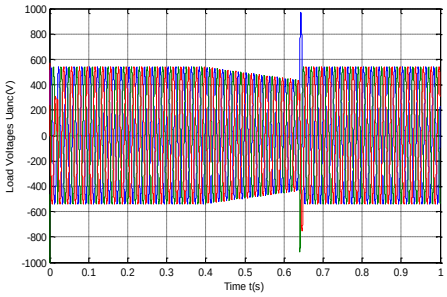

Fig. 22. Load voltage with under load

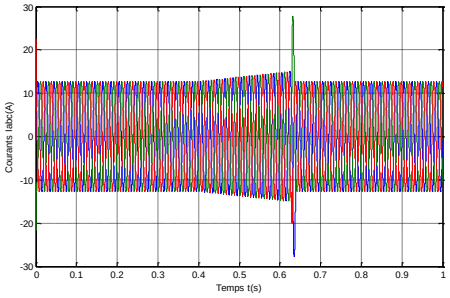

Fig. 23. Load currents with overload

8. Conclusion

In the districts where solar energy and wind energy are naturally complementary, the application of wind-solar hybrid generation system (WSHGS) can reduce the storage capacity of batteries and the total cost of the system compared with stand-alone PV or Wind generation system. In this paper, we have focused on the study of hybrid (photovoltaic wind) systems and the optimization of their energy production and its transfer to low voltage three-phased power grid through power converters with minimum power losses.

The approach adopted in this study consisted on improving the different parts of the power conversion chain as well as the implementation of a protection system to stretch the generators life time and to ensure supplying consumers with electrical energy in case of a grid failure.

References

1. N. Duic and M.G. Carvalho. "*Increasing renewable energy sources in island energy supply: case study Porto Santo*", *Renewable and Sustainable Energy*, Vol. 8, pp. 383-99, 2004.
2. "*Energy Information Administration (EIA)*" (2012) Annual Energy Outlook [online] http://www.eia.gov/countries/country-data.cfm?fips=AG (accessed 12 September 2014).
3. A.B. Stambouli, "*Promotion of renewable energies in Algeria: Strategies and perspectives*", *Renewable and Sustainable Energy Reviews*, Vol. 15, pp. 1169-81, 2011.
4. A.H.M.A. Rahim and E.P. owicki, "*Performance of a grid-connected wind generation system with a robust susceptance controller*", *Electrical Power System Research*, Vol. 81, pp. 149-157, 2011.
5. J.G. Slootweg, S.W.H. De Haan, H. Polinder, and W.L. Kling, "*General model for representing variable speed wind turbines in power system dynamics simulations*", *IEEE Transaction on Power Systems*, Vol. 8, No.1, pp. 144-151, Feb 2003.
6. A. Dahbi, M. Hachemi, N. Nait-Said and M.S. Nait-Said, "*Realization and control of wind turbine*

connected to the grid by using PMSG", *Energy Conversion and management*, Vol. 84, pp. 346-353, 2014.

7. M. Arifujjaman, "*Modelling, simulation and control of grid connected permanent magnet generator (PMG)-based small wind energy conversion system*", Electric Power and Energy Conference (EPEC). IEEE conference publication, pp. 1-6, 2010.
8. L. Ye, H.B. Sun, X.R. Song and L.C. Li, "*Dynamic modeling of hybrid Wind/Solar/Hydro micro grid in EMTP/ATP*", *Renewable Energy*, Vol. 39, pp. 96-106, 2012.
9. A. Safari and S. Mekhilef, "*Simulation and hardware implantation of incremental conductance MPPT with direct control method using cuk converter*", *IEEE Transaction on Industrial Electronics*, Vol. 58, No. 4, pp. 1154-1161, April. 2011.
10. N. Mohan, T. Undeland and W. Robbin, "*Power electronics converters, application and design*", New York: John Wiley & sons, 2003.
11. A. Kirubakaran, J. Shailendra and R.K. Nema, "*The PEM fuel cell system with DC/DC boost converter: design modeling and simulation*", *International Journal of Recent Trends in Engineering*, Vol.1, No.3, May 2009.
12. B.K. Lee and M.A. Ehsani, "*Simplified functional simulation model for three-phase voltage-source inverter using switching function concept*", *IEEE Transaction on Industrial Electronics*, Vol. 48, No. 2, pp. 309-321. April. 2001.
13. A. Masmoudi, A. Abdelkafi and L. Krichen, "*Electric power generation based on variable-speed wind turbine under load disturbance*", *Energy*, Vol. 36, pp. 5016-5026, 2011.
14. B. Indu Rani, C.K. Aravind, G. Saravana Ilango and C. Nagamani, "*A three phase PLL with a dynamic feed forward frequency estimator for synchronization of grid-connected converter under wide frequency variation*", *Electrical Power and Energy Systems*, Vol. 41, pp. 63-70, 2012.
15. I.N. Sotirios and A.P. Stavros, "*Modeling of a PV system with grid code compatibility*", *Electric Power System Research*, Vol. 116, pp. 301-310, 2014.
16. C. Koch-Ciobotaru, R. Boraci, I. Filip, C. Vasar and G. Prostean, "*Control strategy for a variable-speed wind turbine using DC bus measurements. Intelligent system and informatics (SISY)*", *8th international symposium, IEEE conference publication*, pp. 329-334, 2010.
17. M. Turki, J. Belhadj and X. Roboam, "*Control strategy of an autonomous desalination unit fed by PV/Wind hybrid system without battery storage*", *Journal of Electrical System*, Vol. 4, No. 2, pp. 1-12, 2008.
18. Z. Zeng, H. Yang, R. Zhao and C. Cheng, "*Topologies and control strategies of multi-functional grid-connected inverters for power quality enhancement: A comprehensive review*", *Renewable and Sustainable Energy Reviews*, Vol. 24, pp. 223-270, 2013.
19. D. Velasco, C.L. Trujillo, G. Garcera and E. Figueres, "*Review of anti-islanding techniques in distributed generators"*, *Renewable and Sustainable Energy Reviews*, Vol. 14, pp. 1608-1614, 2010.
20. A. Darwish, A.S. Abdel-khalik, A. Elserougi, S. Ahmad and A. Massoud, "*Fault current contribution scenarios for grid-connected voltage source inverter-based distributed generation with an LCL filter*", *Electric Power System Research*, Vol.104, pp. 93-103, 2013.